Preparation and characterization of high value-added activated carbon derived from biowaste walnut shell by KOH activation for supercapacitor electrode

Dawei Lan[1], Mingyan Chen[1,3,*] , Yucheng Liu[1], Qingling Liang[1], Wenwen Tu[1], Yuanyuan Chen[1], Jingjing Liang[1], and Feng Qiu[2]

[1] College of Chemistry and Chemical Engineering, Southwest Petroleum University, Chengdu 610500, Sichuan, China
[2] College of Materials Science and Engineering, Southwest Petroleum University, Chengdu 610500, Sichuan, China
[3] School of Chemistry and Chemical Engineering, Southwest Petroleum University, Chengdu 610500, China

ABSTRACT

Walnut shell, a renewable and easy-accessible agricultural biowaste, was utilized as a precursor for the preparation of activated carbon materials with KOH activation in this study. After a series of activation processes, therefore, the activated carbon derived from walnut shells achieved a specific surface area of 1016.4 m^2/g. With the advantage of low cost and environmental friendly, the prepared carbon materials have superior electrochemical performance and excellent prospects in the application of supercapacitor electrodes. The morphology and textural properties of the AC samples were examined by N_2 adsorption–desorption, scanning electron microscopy, X-ray diffraction, X-ray photoelectron spectroscopy, and FTIR spectra. All the electrode samples exhibited excellent electrochemical performance. The AC-650 electrode achieved a maximum specific capacitance of 169.2 F/g at current density of 0.5 A/g in 6 M KOH electrolyte. This work provided an effective approach for the treatment and utilization of agricultural biowastes, which was worthwhile for economic, environmental, and societal viewpoints.

1 Introduction

Nowadays, more effective energy storage devices are required given huge fossil fuel combustion coupled, and the environmental threat requires the advancement of Industry. Electrochemical capacitor (EC), known as supercapacitors, which is characteristic of long cycle life and large specific power, has drawn growing attention in the energy storage technology field [1]. EC has a wide variety of applications [2] such as digital devices, electrical vehicles, and pulsing techniques [3]. Based on the charge-storage mechanism, there are two categories in the EC, pseudocapacitors, and electric double-layer capacitors (EDLCs) [4]. Supercapacitors store energy by the accumulation of charge in an electric double-layer

that formed at electrodes interface under electrostatic forces, which means that the electrodes play an important role in the storage performance of EDLCs [5, 6].

Generally, Activated carbon (AC) is widely regarded as the first alternative electrode material for EDLCs [7], because of its high specific area and excellent conductivity [8–10]. By virtue of the energy storage mechanism, more studies on the preparation of ordered AC materials were conducted in recent years [11, 12]. The production way of AC can be classified into physical activation [13, 14] and chemical activation [15, 16] typically. The difference is that the activator of physical activation is gas such as CO_2, meanwhile, the activator of chemical activation is chemical agents, such as KOH, $ZnCl_2$, H_3PO_4, and K_2CO_3 [17, 18]. Sometimes chemical activation can be one step, while generally, both the activation methods can involve two steps: the carbonization of raw materials comes first, and then activated at temperatures in the range 500–900 °C [19]. A variety of precursors has been successfully prepared and converted into ACs [20–22]. It is essential to further promote the porosity and specific surface area of AC materials to enhance capacitance, and have a better understanding of the connection between surface chemistry and the performance of EDLCs [23].

Biomass wastes as one type of sustainable, abundant, and environmentally friendly materials showed great potential as AC precursors [24]. Many biomass materials such as waste coffee bean [25], cotton stalk [26], dead leaves [2], nut shells [27], pomelo peels [28], and beer waste [29] have been used as AC materials which are applied for carbon electrodes in supercapacitors with excellent electrochemical performances. The type of precursor materials and activation conditions make a big difference in the electrochemical performance, the surface area, pore size, porous structures, and active surface functional groups of AC electrodes all affect the capacitive performance [30]. This utilization method of biomass wastes can not only provide a new view on energy storage materials but also offer an environmentally friendly approach to take advantage of biomass wastes and generate significant economic valorization [31].

The walnut shell is a nontoxic and stable biowaste material which is mainly composed of lignin, cellulose, and lignocellulose. Due to the high content of carbon, activated carbon prepared from walnut shells

has been studied for some application fields such as adsorption, separation, and wastewater treatment. However, the activated carbon derived from the walnut shell is rarely applied in the energy storage area. With input from industrial and environmental perspectives, activated carbons were prepared from low cost and easy available walnut shells in this work.

2 Experimental

2.1 Materials

The raw walnut shell powder (200 mesh) was obtained from Jie-Kang environmental protection company in Henan province China. Potassium hydroxide (KOH) and hydrochloric acid (HCl) used were of analytical grade without any purification. Distilled water was used for solutions preparation and samples wash. The walnut shell was rinsed with distilled water to remove impurities repeatedly before processing, filtered, and then dried in an oven for 12 h at 105 °C.

2.2 Sample preparation

In this study, a typical one-step chemical activation process was conducted. Firstly, 10 g raw walnut shell was mixed with 100 mL distilled water and 15 g KOH. After stirring for 4 h at room temperature, the mixture was dried at 100 °C in the oven overnight. The obtained product was then pyrolyzed at 10 °C/min heating rate under N_2 atmosphere in the box furnace for 1 h, the final temperature was 650–750 °C. The resulting samples were then washed with diluted HCl solution and deionized water until pH 7. Filtration and dry process were the final steps for sample preparation. AC samples were named AC-X (X = 650, 700, 750), respectively, where X stands for the activation temperature.

2.3 Structural characterization

The AC samples were characterized by N_2 adsorption to analyze the surface area. All the samples were degassed at 300 K for 7 h under vacuum before nitrogen–desorption measurements. The specific surface area was calculated from N_2 Desorption isotherms with the Brunauer–Emmett–Teller (BET)

method. The micropore volume was obtained by the t-plot model for surface analysis. Besides, the Barrett–Joyner–Halenda (BJH) model was utilized to calculate the pore size distribution from the adsorption branches of the isotherms, and the total pore volume was obtained at a relative pressure p/p_0 of 0.99.

Scanning electron microscopy (SEM) was conducted to characterize the morphologies of prepared samples. X-ray diffraction (XRD) measurements were carried out from 5° to 90° (2θ) to investigate the crystallographic information of the AC samples. The surface chemistry of the prepared samples was identified through FTIR spectra measurements. The chemical state of carbon, oxygen, nitrogen elements, and surface chemical composition was investigated by X-ray photoelectron spectroscopy (XPS).

2.4 Electrode preparation and electrochemical measurements

To assess the electrochemical performance of activated carbons, the electrodes were fabricated by mixing AC samples, carbon black, and polytetrafluoroethylene (PTFE, mass percent = 15%) at a mass ratio of 8:1:1. The mixture was stirred with the addition of ethanol to form a homogenous slurry. Then the resultant slurry was pressed onto a nickel foam current collector (1.5 cm × 1 cm). The electrodes were finally prepared after drying at 100 °C for 4 h in an oven. The mass of activated materials was in the range of 10–20 mg.

The electrochemical property was conducted in a typical three-electrode system, in which Platinum foil and Hg/HgO were employed as counter and reference electrodes, and the electrolyte was 6 M KOH aqueous. The electrochemical tests were evaluated on a CHI660D electrochemical workstation by cyclic voltammetry (CV), electrochemical impedance spectra (EIS), and galvanostatic charge–discharge cycles (GC). CV and GC tests were measured at a potential window of 0–1 V, CV tests were carried out at scan rates of 10–100 mV/s, GC cycles were conducted in a current density of 0.5–10 A/g, and EIS tests were measured over the frequency window of 0.01–10 kHz. Finally, 1000 cycles at a current density of 2 A/g under GC were carried out to test the electrochemical stability. The specific gravimetric capacitance of a single electrode derived from the CV tests was calculated according to the following Eq. 1.

$$C_{CV} = \frac{Q}{\Delta V \cdot m},\qquad(1)$$

where C_{CV} (F/g) is the specific capacitance of one single electrode, ΔV is the potential window (V), m is the mass (g) of the active material on the electrode, and Q is the voltammetric charge (C).

The specific gravimetric capacitance of a single electrode was derived from GC tests by Eq. 2.

$$C_{GC} = \frac{I \cdot \Delta t}{m \cdot \Delta V},\qquad(2)$$

where I (A) is the constant current, Δt (s) is the discharge time, m (g) is the mass of active material on the electrode, and ΔV (V) is the voltage ranging from the end of the voltage drop to the end of the discharge process.

3 Results and discussion

3.1 Textural properties

The capacitance performance of AC electrodes materials in supercapacitors has a significant correlation with their specific surface area. Therefore, the test for nitrogen adsorption–desorption was essential. Figure 1a shows the N_2 adsorption and desorption isotherms of all the samples. The isotherms of AC-650 and AC-700 demonstrate that the nitrogen adsorption reached saturation at low pressure, belonging to type I isotherms based on the IUPAC classification, which implies that AC-650 and AC-700 are predominantly microporous. In contrast, AC-750 displays a typical type IV isotherm with a clear H_4-type hysteresis loop at a relative pressure range from 0.3 to 0.9, indicating that this carbon material contains a majority of mesopores. Figure 1b displays the pore size distribution of walnut shell-derived activated carbons. The porosity of AC samples essentially consists of small mesopores (range from 2 to 10 nm). The intrinsic texture of walnut shell might have a bearing on the formation of these mesopores. The pore size distribution also illustrates that macropores in all the AC samples are existent.

Table 1 displayed the pore structure parameters of AC samples prepared from different activation temperatures. It indicates that the influence of activation temperature on the specific surface area of walnut shell-derived carbons is significant. With the increase of temperature from 650 to 750 °C, the specific surface
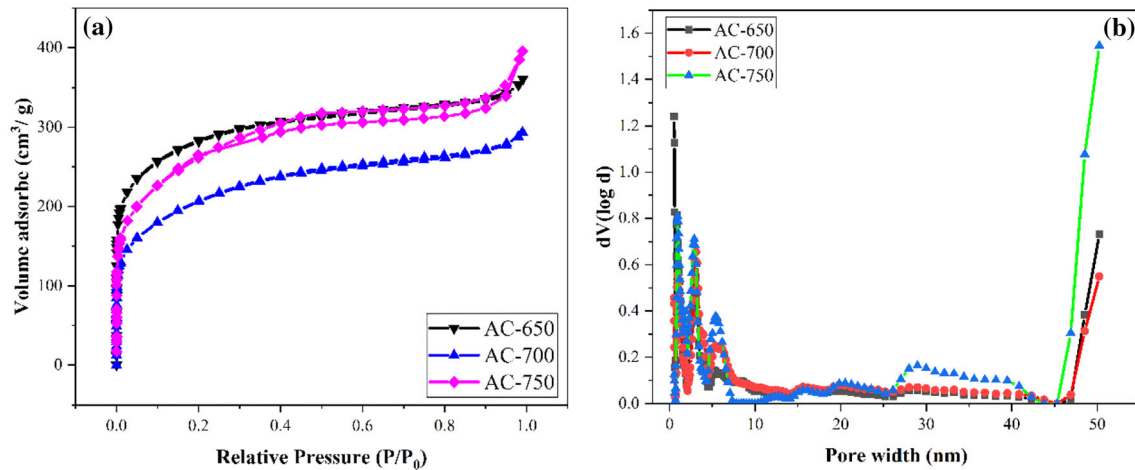
**Fig. 1** **a** Nitrogen adsorption–desorption isotherms and **b** pore size distribution of AC samples

Table 1 The pore structure parameters of AC samples in different activation temperatures

| Samples	S_{BET} (m^2/g)	S_{mic} (m^2/g)	V_{total} (cm^3/g)	V_{mic} (cm^3/g)	V_{mic}/V_{total} (%)	D_a (nm)
AC-650	1016.4	752.9	0.56	0.33	58.9	2.2
AC-700	938.9	618.5	0.61	0.27	44.3	2.6
AC-750	728.2	384.7	0.45	0.17	37.8	2.5

area of AC samples decreased from 1016.4 to 728.2 m^2/g, the micropore surface area decreased from 752.9 to 384.7 m^2/g, and the ratio of micropore volume to total volume decreased from 58.9 to 37.8. At the same time, the average pore size of AC-650, AC-700, and AC-750 are 2.2, 2.6, and 2.5 nm, respectively. It demonstrates that the activation temperature has a great influence on the AC preparation process. When the temperature

exceeded a critical point, the micropores began to collapse and the small mesopores formed [32]. On the whole, all the AC samples have a relatively large surface area and developed pore structure, providing a lot of ion adsorption sites for electric double-layer and interconnected ion-diffusion pathways [5].
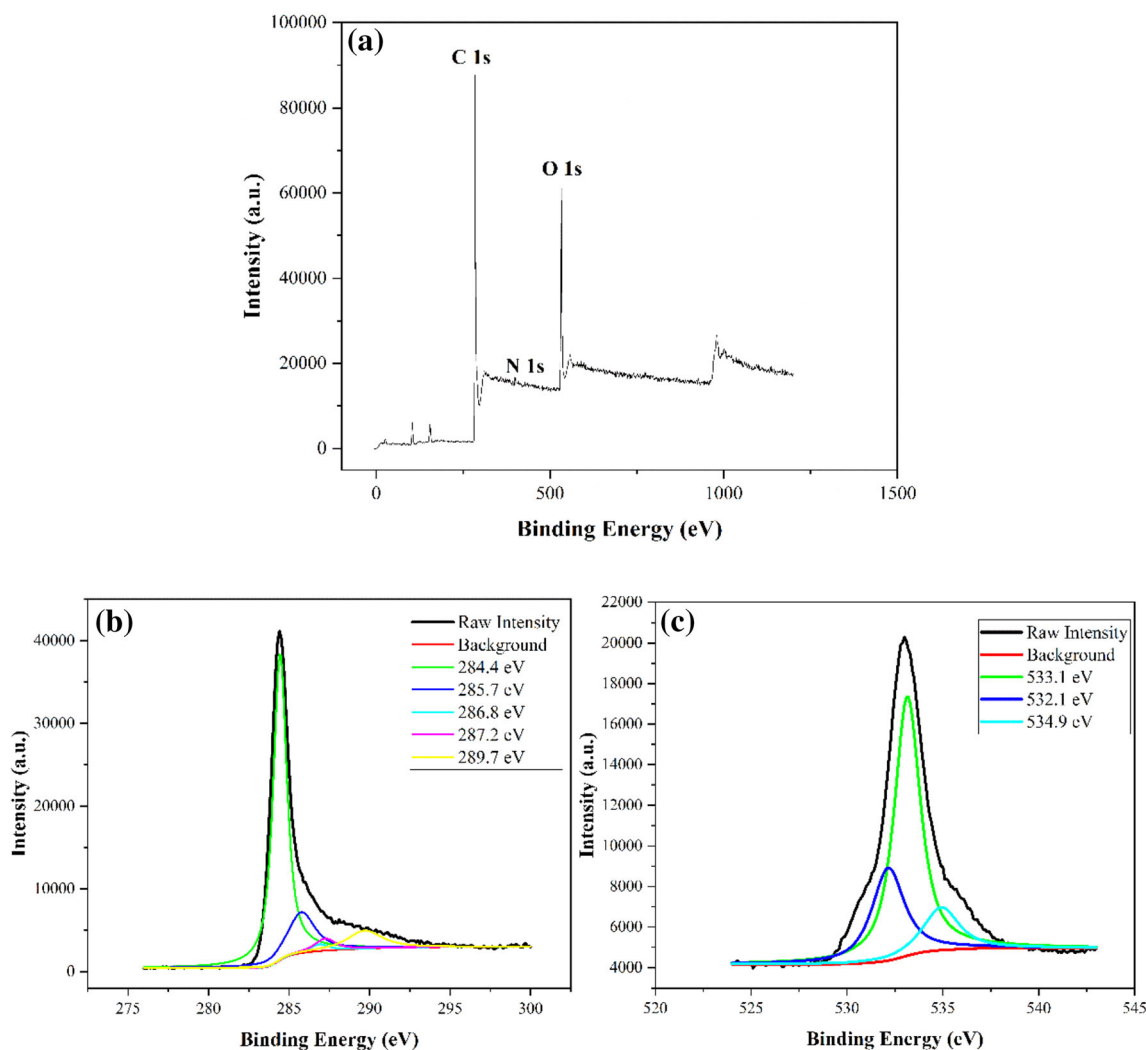
Figure 2a displays the XRD patterns of all the AC materials derived from the walnut shell, there are
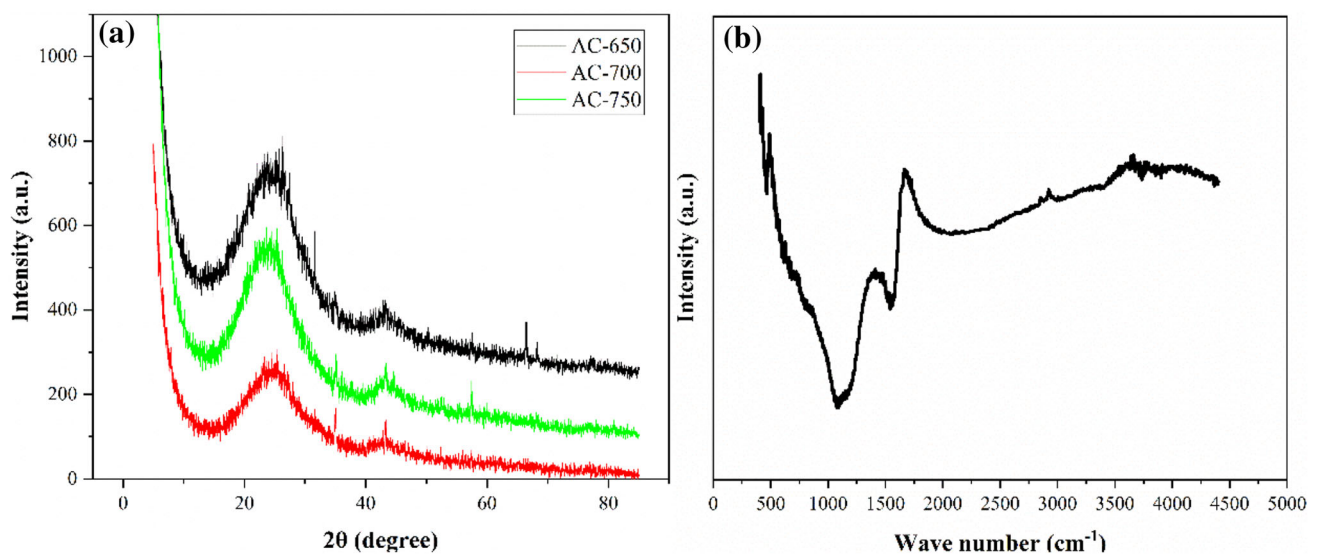
Fig. 2 XRD patterns (**a**) of all AC samples and FTIR spectra (**b**) of AC-650
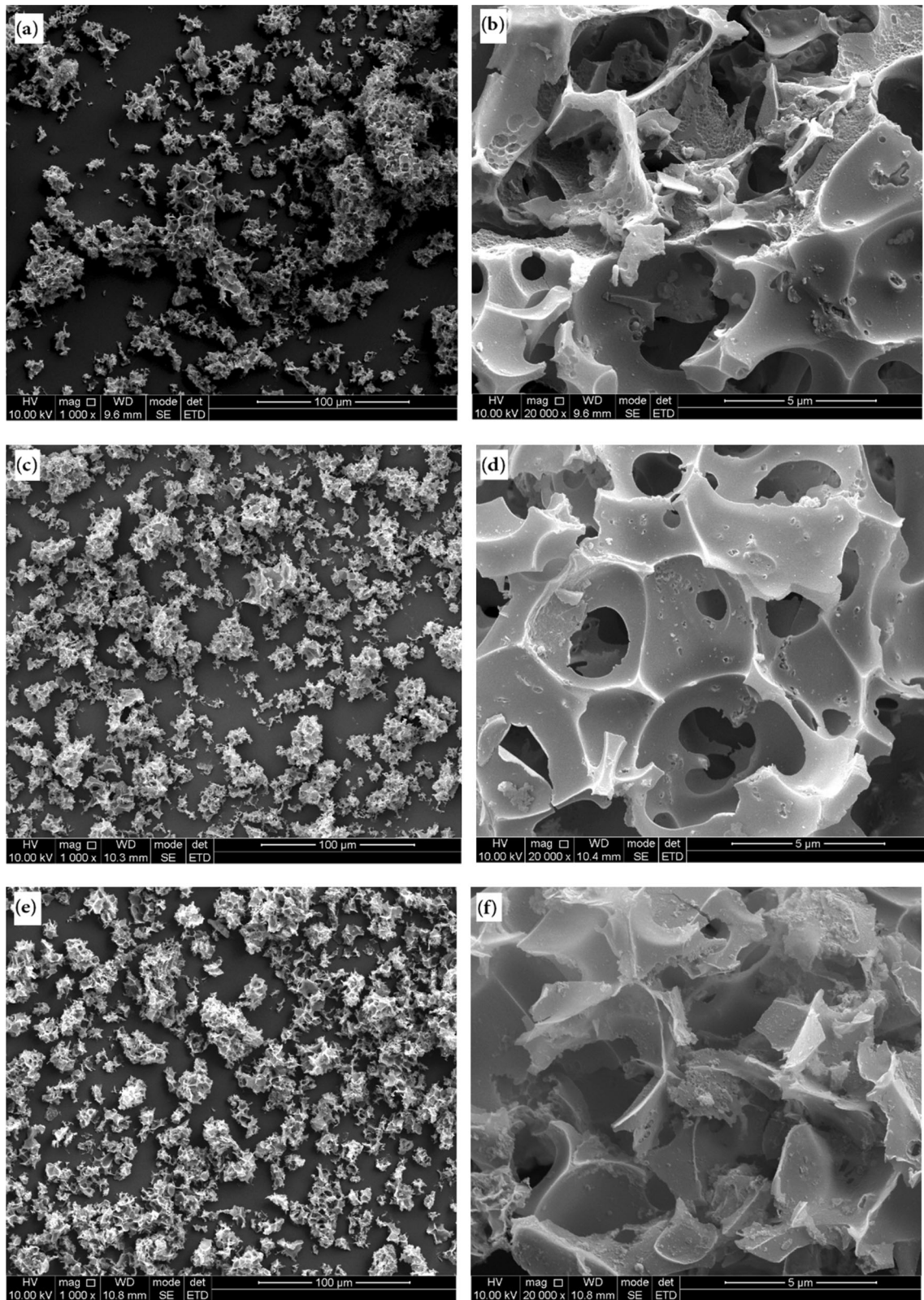
Fig. 3 SEM images of AC-650 (**a**, **b**); SEM images of AC-700 (**c**, **d**); SEM images of AC-750 (**e**, **f**)

Fig. 4 XPS spectra (**a**), C 1s (**b**), O 1s (**c**), and core-level spectra of AC-650

two diffraction peaks observed at about 22° and 44° in all the samples, which can be indexed as the (1 0 0) and (0 0 2) graphitic planes, implying that each sample contains amorphous carbon [33]. The FTIR spectra in Fig. 2b show that AC-650 is composed of several functional groups. The peak in the region of 3500–3600 cm^{-1} could be ascribed to the O–H stretching from the hydroxylic groups and adsorbed moisture. The peaks appearing at about 1650 cm^{-1} are associated with the presence of –C=O stretching vibration of carbonyl groups. In addition, the sharp peak at about 1380 cm^{-1} is attributed to the C–H bonds, which is originated from the hydrochloric acid used for the neutralization of KOH (activation agent) in the AC samples.

SEM tests were used to observe the microscopic morphology of AC materials derived from walnut shells. Figure 3 shows the SEM images of AC-650, AC-700, and AC-750. The SEM images demonstrate that each sample was filled with hollow tunnels, ascribing to the gasification of volatiles after activation. All the AC samples were composed of high-quality particles in agglomeration. What is more, it could be observed that the carbon particles in every sample were disordered/turbostratic, which was consistent with the results of XRD analysis.

XPS tests were used to measure the components and chemical bonding of AC samples. Figure 4a displays the XPS spectrum generated from AC-650, which exhibits a predominant C 1s peak, an O 1s peak, and a weak N 1s peak. The carbon, oxygen, and nitrogen contents of AC-650 are 76.83%, 22.54% and 0.63%, respectively, calculated from XPS tests. It can be seen obviously that carbon and oxygen elements
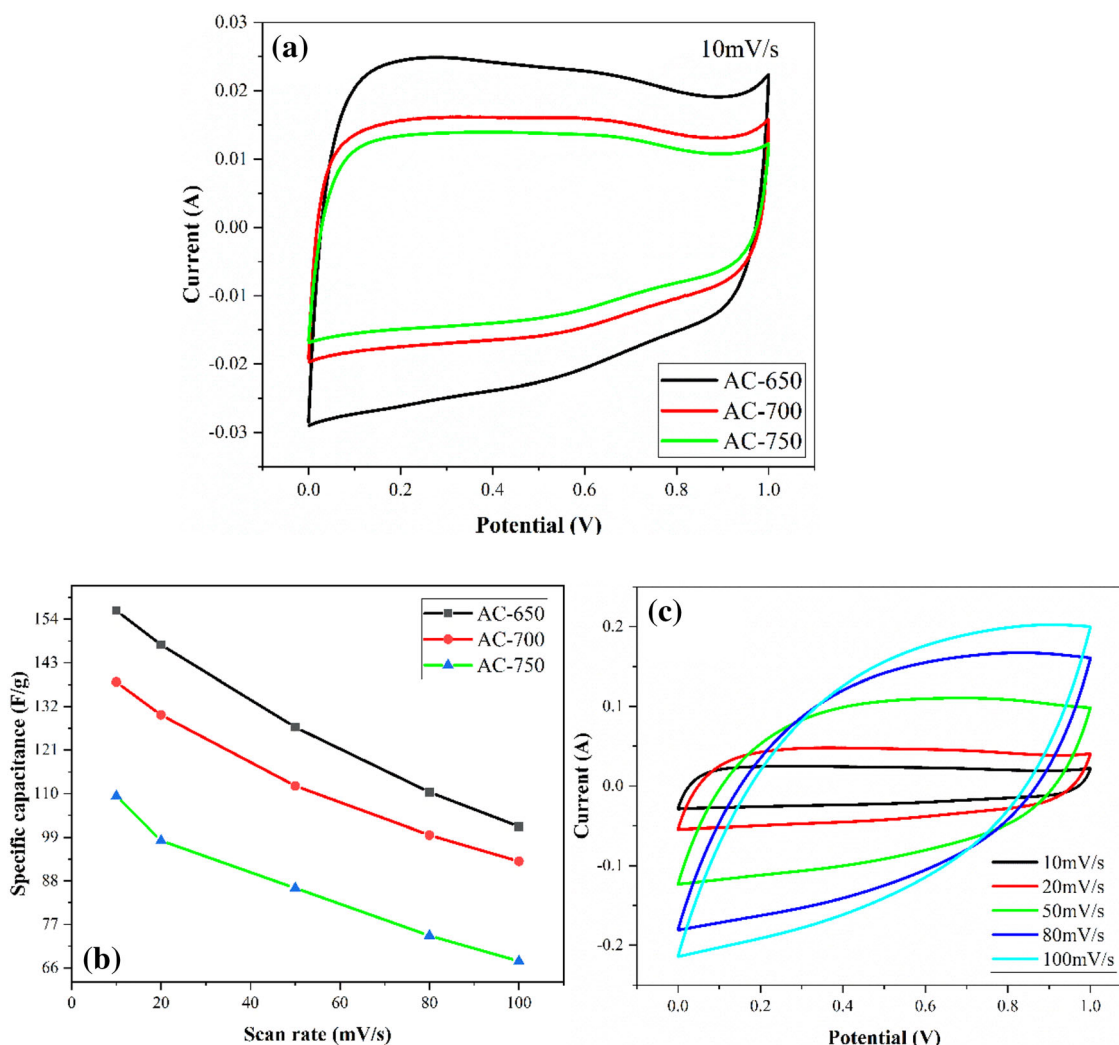
Fig. 5 **a** CV curves of AC-650, AC-700, and AC-750 at a scan rate of 10mv/s; **b** plot of specific capacitance of AC-650, AC-700, and AC-750; **c** CV curves of AC-650 at different scan rates

are the main moieties of the AC sample. The high resolution of C 1s spectra for AC-650 is shown in Fig. 4b. There are five sub-peaks deconvoluted from the C 1s peak, the main peak centered at 284.4 eV corresponds to conjugated C=C sp^2 hybridized bonds [34]. The secondary peak at 285.7 eV is ascribed to the existence of C–C sp^3 hybridized bonds. The peaks located at 286.8 eV, 287.2 eV, and 289.7 eV can be attributed to the presence of C–O/C–N, C=O/C=N, and O=C–O, respectively [35]. The O 1s core-level spectrum of AC-650 is shown in Fig. 4c. As shown in the picture, the peak at 533.1 eV is attributed to C–O–H and C–O–C bonds. The peak appearing at 532.1 eV corresponds to phenol groups. What is more, the peak at 534.9 eV is attributed to COOH and HOH

bonds. The coexistence of all these functional groups can enhance the capacitance of AC samples [36].

3.2 Electrochemical studies

The typical CV curves of AC samples AC-650, AC-700, AC-750 at a scan rate of 10 mv/s are exhibited in Fig. 5a. All the CV curves exhibit quasi-rectangular shape with slightly distorted, which indicates the generation of typical electrical double layer in aqueous electrolyte (6 M KOH) and equivalent series resistance (ESR) in every electrode [37]. At the same time, there was no significant redox signal in all CV curves, meaning the absence of pseudocapacitance in this charge-storage mechanism. The ion diffusion rate in the pores of the electrodes can be conjectured from
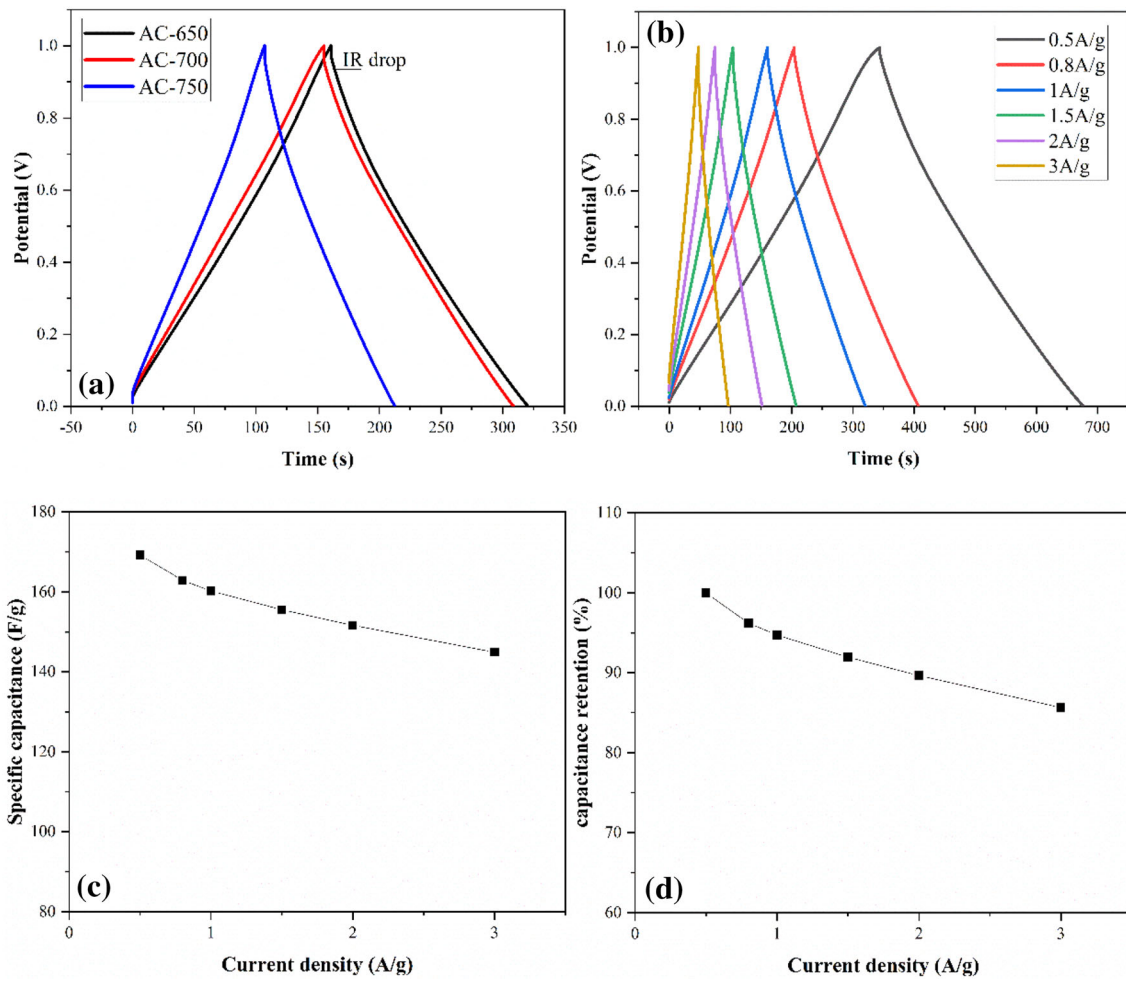
Fig. 6 a GC curves of AC samples at 1 A/g; **b** GC curves of AC-650 at different current densities; **c** influence of current density on the specific capacitance of AC-650, **d** influence of current density on capacitance retention of AC-650

Table 2 Comparison of AC derived from different precursors

Precursor	Activation method	S_{BET} (m^2/g)	Capacitance (F/g)	Electrolyte	Ref.
Walnut shell	KOH	1016	169	6 M KOH	This work
Rice husk	KOH	2696	147	6 M KOH	[32]
Pistachio shell	KOH	1009	125	1 M HNO$_3$	[41]
Fir wood	Steam	1130	142	1 M HNO$_3$	[42]
Cotton stalk	H$_3$PO$_4$	1481	114	1 M TEABF$_4$	[43]
Beer lees	KOH	3560	188	0.1 M H$_2$SO$_4$	[44]
Scrap waste tire	H$_3$PO$_4$	510	93	6 M KOH	[45]
Sugar cane bagasse	NaOH	2871	109	1 M H$_2$SO$_4$	[46]
Fir wood	Steam	1016	110	0.5 M H$_2$SO$_4$	[41]
Fir wood	KOH	1064	180	0.5 M H$_2$SO$_4$	[41]

Fig. 7 Nyquist plot of AC-650
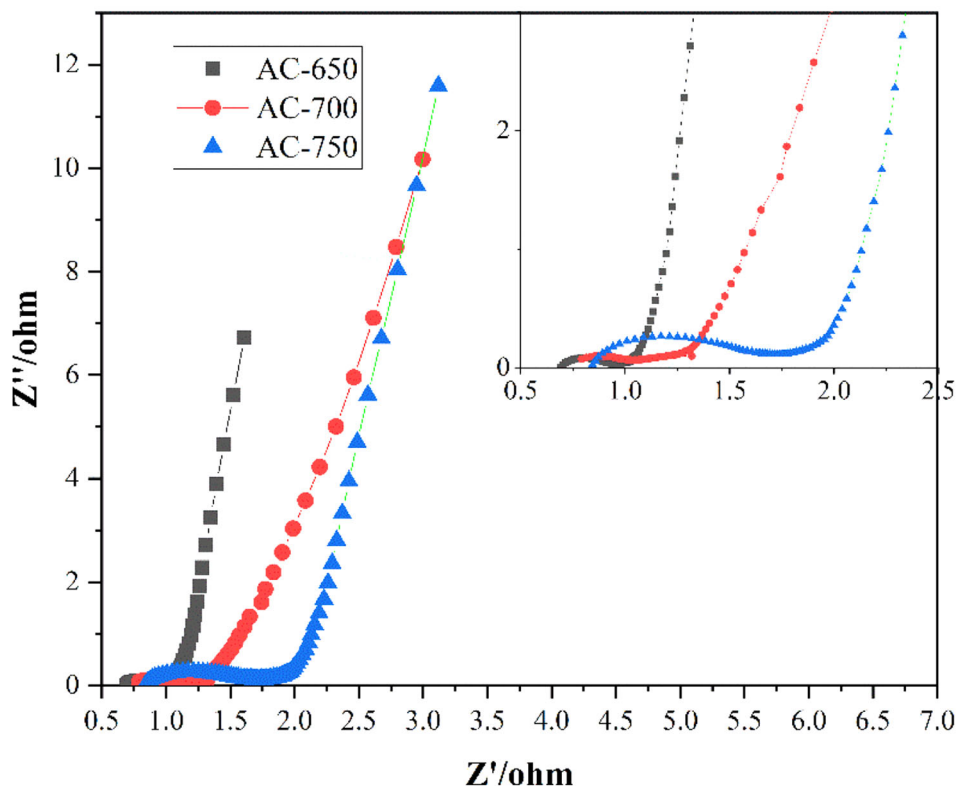
the rectangular degree of the CV curves, which means that the rectangular degree is positively correlated with the ion diffusion rate. Consequently, the quasi-rectangular shape of all the CV curves in Fig. 5a shows that every electrode performed a fast speed ion diffusion and excellent charge propagation at a relatively low scan rate [38].

The specific capacitances of AC electrodes at different scan rates were calculated from the CV curves shown in Fig. 5b. The maximum specific capacitance values of AC-650, AC-700, AC-750 were performed at 10 mV/s and, respectively, computed as 156.19 F/g, 138.15 F/g, and 109.76 F/g. Figure 5b demonstrates that the specific capacitance of all three electrodes declines with the raise of scan rates, which is consistent with the previous studies, ascribing to diffusion limitation. Considering rate capability is a significant factor for electrode materials in supercapacitors, Fig. 5c shows the CV tests of AC-650 electrode at diverse scan rates ranging from 10 to 100 mV/s, just as shown in Fig. 5c, with the amplification of scan rates, a certain extent of distortion occurred, but the CV curves still retained rectangular-like shape even at a high scan rate. At the same time, the capacitance of AC-650 is maintained at

101.70 F/g when the scan rate increased to 100 mv/s, the capacitance retention is 65.11%. The similarity of the CV curves at different scan rates indicates that a preeminent high-rate capacitive behavior existed within the electrode material [39].

Figure 6a depicts typical GC curves of activated carbon electrodes at 1 A/g current density. Each GC curve is highly symmetric and linear with a slight IR drop. The curves suggest great reversibility and high coulombic efficiency as electrodes for supercapacitors. The IR drop may result from ionic transport obstruction at the elevated potential. At the same time, the slight drop indicates that each electrode presents a low internal series resistance. A longer charge–discharge time typically indicates a higher specific capacitance value [40]. The AC-650 electrode has the best specific capacitance among all samples, which is consistent with the CV result shown before. Therefore, GC tests of AC-650 electrode at diverse current densities from 0.5 to 3 A/g were conducted, which is shown in Fig. 6b. The GC curve at each current density presents a similar isosceles triangular shape, implying that the AC-650 electrode has excellent electrochemical reversibility and conductivity.

The specific capacitance values of AC-650 calculated from discharging curves are summarized in Fig. 6c. The specific capacitances at 0.5, 0.8, 1, 1.5, 2, and 3 A/g are 169.2, 162.92, 160.29, 155.58, 151.68, and 144.92 F/g, respectively. The specific capacitance declines from 169.2 F/g to 144.92 F/g with increase in the current density from 0.5 A/g to 3A/g. The lower current density indicates higher specific capacitance. This is due to the faster diffusion and migration of ions at lower current density through the electrodes. Furthermore, the capacitance retention of AC-650 is displayed in Fig. 6d, the specific capacitance could retain as high as 85.65% when the current density reached 3 A/g, implying excellent rate performance. The electrochemical performances of AC samples in this study and AC materials prepared from various precursors are compared in Table 2.

To evaluate the charge kinetic properties of AC electrodes, electrochemical impedance spectroscopy (EIS) tests were conducted in 6 M KOH electrolyte at the frequency ranging from 0.01 Hz to 10 kHz, and the alternate current amplitude is 5 mV. Figure 7 displays the Nyquist curves of AC electrodes at open-circuit voltage. The Nyquist plot of a typical AC electrode can be divided into two distinct parts: one is a semicircle part of high frequency, and the other is a linear part in low frequency [47]. As shown in Fig. 7, each plot performs an excellent Nyquist curve of a typical AC electrode just as one previous study [48]. The intersection of the x-axis at the high frequency is known as the equivalent series resistance (ESR), determining the power capability for a supercapacitor. Every electrode was found to be a low internal resistance, which is 0.6, 0.7, and 0.9 Ω for AC-650, AC-700, and AC-750, respectively. The low ESR can be ascribed to the high electron conductivity of the local graphitized framework. At the same time, the ESR values can be concluded in the order of AC-650 > AC-700 > AC-750. The semicircle in high frequency could be ascribed to the reason that double-layer capacitance parallel with faradaic reactions charge-transfer resistance (Rct) [49]. According to previous study, the impedance for the tested electrode which increased with the semicircle diameter is closely related. As displayed in Fig. 7, the order of impedance is just the same as ESR values. With the decrease of frequency, each curve of the AC electrode presents an inclined line and is almost vertical to the y-axis. The nearly vertical line at low-frequency range has a bearing on the diffusion of the ions within the supercapacitors system, or called Warburg impedance [50]. A higher phase angle means a lower

Fig. 8 Stability test for AC-650 at 2 A/g for 1000 cycles
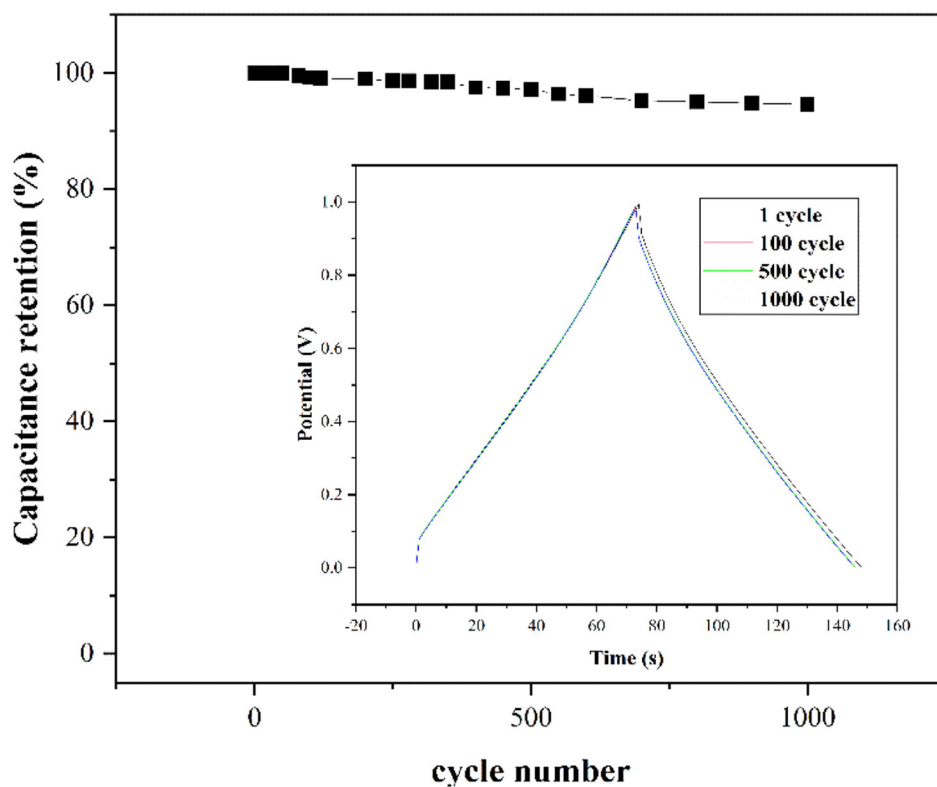
Warburg impedance, so AC-650 < AC-700 < AC-750, in the term of Warburg impedance. It could be attributed to the high porosity and high surface area of AC-650 which is better than others. The nearly theoretical vertical lines of AC electrodes indicate excellent diffusion of the electrolyte into the electrodes in the system [2].

Long cycle life is another essential concern for the application of supercapacitors. The electrochemical stability of the AC-650 electrode was evaluated under GCD tests for 1000 cycles at a current density of 2 A/g, which is shown in Fig. 8. It can be seen that there is only a slight decline in specific capacitance after 1000 cycles. AC-650 electrode can retain approximately 94.6% of its capacitance. The gradual decay could be ascribed to the block of the micropores on the AC electrode after the continuous cycle process. Such blockage could reduce ions adsorption, and decrease the specific capacitance. Therefore, the capacitance retention performance of AC-650 indicates that the AC electrode exhibits excellent electrochemical cycling stability.

4 Conclusions

In summary, high value-added AC materials derived from walnut shell have been fabricated under different temperatures with KOH activation for supercapacitor electrode. As a cheap, sustainable, and environmental-friendly resource, the walnut shell would be a promising precursor for the industrial production of high-quality activated carbon at a high efficiency/cost ratio. Structural characterizations display that all the AC samples possess large surface areas and moderate mesoporosities. Electrochemical measurements illustrate that the samples have excellent electrochemical performance. The optimum sample is AC-650, which exhibited the highest specific surface area and the best electrochemical performance. The specific surface area of AC-650 is 1016.4 m^2/g, and the total pore volume is 0.56 cm^3/g. The AC-650-based electrode for supercapacitor possesses a high specific capacitance of 169.2 F/g at 0.5 A/g. The electrochemical findings in this study indicate that the walnut shell, as a cheap, sustainable, and environmental-friendly resource, is a promising suitable precursor to fabricate activated carbon for the supercapacitor electrode.

References

1. R. Kötz, M. Carlen, Principles and applications of electrochemical capacitors. Electrochim. Acta 45, 2483–2498 (2000)
2. M. Biswal, A. Banerjee, M. Deo, S. Ogale, From dead leaves to high energy density supercapacitors. Energy Environ. Sci. 6, 1249–1259 (2013)
3. W. Xing, S.Z. Qiao, R.G. Ding, F. Li, G.Q. Lu, Z.F. Yan, H.M. Cheng, Superior electric double layer capacitors using ordered mesoporous carbons. Carbon 44, 216–224 (2006)
4. Y. Tian, S. Cong, W. Su, H. Chen, Q. Li, F. Geng, Z. Zhao, Synergy of W18O49 and polyaniline for smart supercapacitor electrode integrated with energy level indicating functionality. Nano Lett. 14, 2150–2156 (2014)
5. P. Simon, Y. Gogotsi, Materials for electrochemical capacitors. Nat. Mater. 7, 845 (2008)
6. P. Simon, Y. Gogotsi, B. Dunn, Where do batteries end and supercapacitors begin? Science 343, 1210 (2014)
7. L.L. Zhang, X.S. Zhao, Carbon-based materials as supercapacitor electrodes. Chem. Soc. Rev. 38, 2520–2531 (2009)
8. S. Zhang, N. Pan, Supercapacitors performance evaluation. Adv. Energy Mater. 5, 1401401 (2015)
9. G.P. Pandey, A.C. Rastogi, C.R. Westgate, All-solid-state supercapacitors with poly(3,4-ethylenedioxythiophene)-coated carbon fiber paper electrodes and ionic liquid gel polymer electrolyte. J. Power Sources 245, 857–865 (2014)
10. H. Jiang, P.S. Lee, C. Li, 3D carbon based nanostructures for advanced supercapacitors. Energy Environ. Sci. 6, 41–53 (2013)
11. F. Béguin, V. Presser, A. Balducci, E. Frackowiak, Carbons and electrolytes for advanced supercapacitors. Adv. Mater. 26, 2219–2251 (2014)
12. J. Jiang, L. Zhang, X. Wang, N. Holm, K. Rajagopalan, F. Chen, S. Ma, Highly ordered macroporous woody biochar with ultra-high carbon content as supercapacitor electrodes. Electrochim. Acta 113, 481–489 (2013)
13. A. Ahmadpour, D.D. Do, The preparation of active carbons from coal by chemical and physical activation. Carbon 34, 471–479 (1996)
14. Y. Zou, B. Han, High-surface-area activated carbon from Chinese coal. Fuel Energy Abstr. 43, 252 (2002)

15. M.A. Lillo-Ródenas, D. Cazorla-Amorós, A. Linares-Solano, Understanding chemical reactions between carbons and NaOH and KOH: an insight into the chemical activation mechanism. Carbon **41**, 267–275 (2003)

16. M. Molina-Sabio, F. RodRíguez-Reinoso, F. Caturla, M.J. Sellés, Porosity in granular carbons activated with phosphoric acid. Carbon **33**, 1105–1113 (1995)

17. W.T. Tsai, C.Y. Chang, S.L. Lee, A low cost adsorbent from agricultural waste corn cob by zinc chloride activation. Bioresour. Technol. **64**, 211–217 (1998)

18. R. Baccar, J. Bouzid, M. Feki, A. Montiel, Preparation of activated carbon from Tunisian olive-waste cakes and its application for adsorption of heavy metal ions. J. Hazard. Mater. **162**, 1522–1529 (2009)

19. W. Li, L.-B. Zhang, J.-H. Peng, N. Li, X.-Y. Zhu, Preparation of high surface area activated carbons from tobacco stems with K_2CO_3 activation using microwave radiation. Ind. Crops Prod. **27**, 341–347 (2008)

20. Ç. Şentorun-Shalaby, M.G. Uçak-Astarlıoğlu, L. Artok, C. Sarıcı, Preparation and characterization of activated carbons by one-step steam pyrolysis/activation from apricot stones. Microporous Mesoporous Mater. **88**, 126–134 (2006)

21. M.L. Martínez, M.M. Torres, C.A. Guzmán, D.M. Maestri, Preparation and characteristics of activated carbon from olive stones and walnut shells. Ind. Crops Prod. **23**, 23–28 (2006)

22. H. Deng, L. Yang, G. Tao, J. Dai, Preparation and characterization of activated carbon from cotton stalk by microwave assisted chemical activation—application in methylene blue adsorption from aqueous solution. J. Hazard. Mater. **166**, 1514–1521 (2009)

23. A.M. Abioye, Z.A. Noorden, F.N. Ani, Synthesis and characterizations of electroless oil palm shell based-activated carbon/nickel oxide nanocomposite electrodes for supercapacitor applications. Electrochim. Acta **225**, 493–502 (2017)

24. H. Wang, Z. Xu, A. Kohandehghan, Z. Li, K. Cui, X. Tan, T.J. Stephenson, C.K. King'Ondu, C.M. Holt, B.C. Olsen, J.K. Tak, D. Harfield, A.O. Anyia, D. Mitlin, Interconnected carbon nanosheets derived from hemp for ultrafast supercapacitors with high energy. ACS Nano **7**, 5131–5141 (2013)

25. T.E. Rufford, D. Hulicova-Jurcakova, Z. Zhu, G.Q. Lu, Nanoporous carbon electrode from waste coffee beans for high performance supercapacitors. Electrochem. Commun. **10**, 1594–1597 (2008)

26. M. Chen, X. Kang, T. Wumaier, J. Dou, B. Gao, Y. Han, G. Xu, Z. Liu, L. Zhang, Preparation of activated carbon from cotton stalk and its application in supercapacitor. J. Solid State Electrochem. **17**, 1005–1012 (2013)

27. J. Xu, Q. Gao, Y. Zhang, Y. Tan, W. Tian, L. Zhu, L. Jiang, Preparing two-dimensional microporous carbon from

28. K.-L. Hong, L. Qie, R. Zeng, Z.-Q. Yi, W. Zhang, D. Wang, W. Yin, C. Wu, Q.-J. Fan, W.-X. Zhang, Y.-H. Huang, Biomass derived hard carbon used as a high performance anode material for sodium ion batteries. J. Mater. Chem. A **2**, 12733–12738 (2014)

29. W. Hao, N. Keshavarzi, A. Branger, L. Bergström, N. Hedin, Strong discs of activated carbons from hydrothermally carbonized beer waste. Carbon **78**, 521–531 (2014)

30. J.R. Miller, P. Simon, Electrochemical capacitors for energy management. Science **321**, 651 (2008)

31. A.M. Abioye, F.N. Ani, Recent development in the production of activated carbon electrodes from agricultural waste biomass for supercapacitors: a review. Renew. Sustain. Energy Rev. **52**, 1282–1293 (2015)

32. E.Y.L. Teo, L. Muniandy, E.-P. Ng, F. Adam, A.R. Mohamed, R. Jose, K.F. Chong, High surface area activated carbon from rice husk as a high performance supercapacitor electrode. Electrochim. Acta **192**, 110–119 (2016)

33. W. Lv, F. Wen, J. Xiang, J. Zhao, L. Li, L. Wang, Z. Liu, Y. Tian, Peanut shell derived hard carbon as ultralong cycling anodes for lithium and sodium batteries. Electrochim. Acta **176**, 533–541 (2015)

34. Y. Li, W. Zhou, H. Wang, L. Xie, Y. Liang, F. Wei, J.-C. Idrobo, S.J. Pennycook, H. Dai, An oxygen reduction electrocatalyst based on carbon nanotube–graphene complexes. Nat. Nanotechnol. **7**, 394 (2012)

35. Y.J. Kim, Y. Abe, T. Yanagiura, K.C. Park, M. Shimizu, T. Iwazaki, S. Nakagawa, M. Endo, M.S. Dresselhaus, Easy preparation of nitrogen-enriched carbon materials from peptides of silk fibroins and their use to produce a high volumetric energy density in supercapacitors. Carbon **45**, 2116–2125 (2007)

36. Y. Ma, C. Ma, J. Sheng, H. Zhang, R. Wang, Z. Xie, J. Shi, Nitrogen-doped hierarchical porous carbon with high surface area derived from graphene oxide/pitch oxide composite for supercapacitors. J. Colloid Interface Sci. **461**, 96–103 (2016)

37. M.D. Stoller, S. Park, Y. Zhu, J. An, R.S. Ruoff, Graphene-based ultracapacitors. Nano Lett. **8**, 3498–3502 (2008)

38. E. Frackowiak, F. Béguin, Carbon materials for the electrochemical storage of energy in capacitors. Carbon **39**, 937–950 (2001)

39. J.Q. Shi, Z.P. Zhao, J.C. Wu, Y.B. Yu, Z.K. Peng, B.J. Li, Y.S. Liu, H.W. Kang, Z.Y. Liu, Synthesis of aminopyrene-tetraone-modified reduced graphene oxide as an electrode material for high-performance supercapacitors. ACS Sustain. Chem. Eng. **6**, 4729–4738 (2018)

40. K. Chaitra, R.T. Vinny, P. Sivaraman, N. Reddy, C.Y. Hu, K. Venkatesh, C.S. Vivek, N. Nagaraju, N. Kathyayini, KOH

Pistachio nutshell with high areal capacitance as supercapacitor materials. Sci. Rep. **4**, 5545 (2014)

activated carbon derived from biomass-banana fibers as an efficient negative electrode in high performance asymmetric supercapacitor. J. Energy Chem. **26**, 56–62 (2017)

41. F.-C. Wu, R.-L. Tseng, C.-C. Hu, C.-C. Wang, Effects of pore structure and electrolyte on the capacitive characteristics of steam- and KOH-activated carbons for supercapacitors. J. Power Sources **144**, 302–309 (2005)

42. R. Farma, M. Deraman, A. Awitdrus, I.A. Talib, E. Taer, N.H. Basri, J.G. Manjunatha, M.M. Ishak, B.N.M. Dollah, S.A. Hashmi, Preparation of highly porous binderless activated carbon electrodes from fibres of oil palm empty fruit bunches for application in supercapacitors. Bioresour. Technol. **132**, 254–261 (2013)

43. T. Adinaveen, L. John Kennedy, J. Judith Vijaya, G. Sekaran, Surface and porous characterization of activated carbon prepared from pyrolysis of biomass (rice straw) by two-stage procedure and its applications in supercapacitor electrodes. J. Mater. Cycles Waste Manage. **17**, 736–747 (2015)

44. R. Abd Aziz, I.I. Misnon, K.F. Chong, M.M. Yusoff, R. Jose, Layered sodium titanate nanostructures as a new electrode for high energy density supercapacitors. Electrochim. Acta **113**, 141–148 (2013)

45. P. Zhao, Y. Han, X. Dong, C. Zhang, S. Liu, Application of activated carbons derived from scrap tires as electrode materials for supercapacitors. ECS J. Solid State Sci. Technol. **4**, M35–M40 (2015)

46. K. Konno, Y. Ohba, K. Onoe, T. Yamaguchi, Preparation of activated carbon having the structure derived from biomass by alkali activation with NaOH, and its application in electric double-layer capacitors. Carbon **46**, 721 (2008)

47. C. Portet, P.L. Taberna, P. Simon, E. Flahaut, C. Laberty-Robert, High power density electrodes for carbon supercapacitor applications. Electrochim. Acta **50**, 4174–4181 (2005)

48. X. Gao, W. Xing, J. Zhou, G. Wang, S. Zhuo, Z. Liu, Q. Xue, Z. Yan, Superior capacitive performance of active carbons derived from Enteromorpha prolifera. Electrochim. Acta **133**, 459–466 (2014)

49. M.X. Liu, L.H. Gan, W. Xiong, F.Q. Zhao, X.Z. Fan, D.Z. Zhu, Z.J. Xu, Z.X. Hao, L.W. Chen, Nickel-doped activated mesoporous carbon microspheres with partially graphitic structure for supercapacitors. Energy Fuels **27**, 1168–1173 (2013)

50. X. Du, W. Zhao, Y. Wang, C. Wang, M. Chen, T. Qi, C. Hua, M. Ma, Preparation of activated carbon hollow fibers from ramie at low temperature for electric double-layer capacitor applications. Bioresour. Technol. **149**, 31–37 (2013)